

# 2–d stability of the Néel wall

Antonio DeSimone\*, Hans Knüpfer†, Felix Otto†

November 23, 2006

## Abstract

We are interested in thin–film samples in micromagnetism, where the magnetization  $m$  is a 2–d unit–length vector field. More precisely we are interested in transition layers which connect two opposite magnetizations, so called Néel walls.

We prove stability of the 1–d transition layer under 2–d perturbations. This amounts to the investigation of the following singularly perturbed energy functional:

$$E_{2d}(m) = \epsilon \int |\nabla m|^2 dx + \frac{1}{2} \int |\nabla^{-1/2} \nabla \cdot m|^2 dx.$$

The topological structure of this two–dimensional problem allows us to use a duality argument to infer the optimal lower bound. The lower bound relies on an  $\epsilon$ –perturbation of the following *logarithmically failing* interpolation inequality

$$\int |\nabla^{1/2} \phi|^2 dx \not\lesssim \sup |\phi| \int |\nabla \phi| dx.$$

**Mathematical subject classification:** 78A30, 49S05, 78A99, 49K20

## 1 Introduction and motivation

### 1.1 Micromagnetic energy

The non–dimensionalized magnetization of a ferromagnetic sample  $\Omega \subset \mathbb{R}^3$  can be described by a unit vector field  $m : \Omega \rightarrow S^2$ . The micromagnetic model states that experimentally observed magnetizations are (local) minimizers of the following energy functional:

$$E_{3d}(m) = d^2 \int_{\Omega} |\nabla m|^2 dx + \int_{\mathbb{R}^3} |\nabla u|^2 dx. \quad (1)$$

---

\*SISSA, International School for Advanced Mathematics, Via Beirut 2–4, 34014 Trieste, Italy

†Institute of Applied Mathematics, University of Bonn, Wegelerstrasse 10, 53115 Bonn, Germany

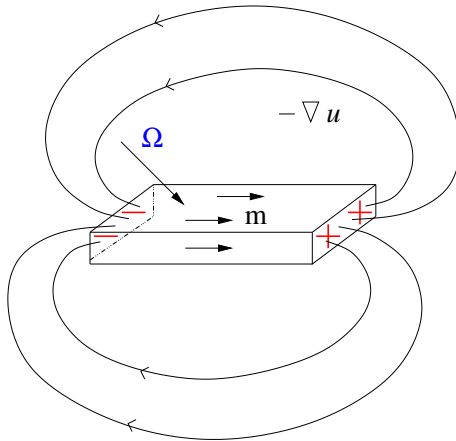


Figure 1: Surfaces charges generating a stray field

The first term is called exchange energy, the second stray field energy, see [11, p. 148] for the physics. The stray field potential  $u : \mathbb{R}^3 \rightarrow \mathbb{R}$  is determined by

$$\Delta u = \nabla \cdot m, \quad (2)$$

where we think of  $m$  as being extended by 0 outside  $\Omega$ . Therefore the stray field is generated by both divergence of  $m$  inside the magnetic sample (“volume charges”) and a non-zero tangential component of  $m$  on the surface of the magnetic sample (“surface charges”), see Figure 1. The material constant  $d$  is called exchange length. We do not include anisotropy and external fields.

In magnetic samples large uniformly magnetized regions are observed (“magnetic domains”). These are separated by narrow transition layers (“domain walls”), where the magnetization vectors varies rapidly.

## 1.2 A mesoscopic view: Why domain walls in films?

In bulk samples, crystalline anisotropy is necessary for the formation of domains. This is not the case for films as we shall explain now, following van den Berg [19].

Because of the film geometry, the exchange energy does not leave much room for variations in the thickness direction  $x_3 \in (0, t)$ . Let us assume that this turns into the constraint that on the mesoscopic level  $m$  only depends on in-plane variables, i.e.

$$m = m(x').$$

Here and in the sequel, the prime always indicates an in-plane quantity. Surface charges, i. e.  $m \cdot \nu$ , generate a stray field. In a thin-film sample, there is a lot of surface:  $\Omega' \times \{0, t\}$ . Hence the  $m_3$ -component is strongly penalized. We assume  $m_3 \equiv 0$  on the mesoscopic level. Hence

$$m = m'(x')$$

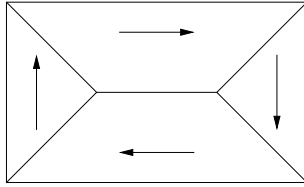


Figure 2: Landau State

is a 2-d vector field. The stray-field energy also penalizes the normal component at the lateral boundary  $\partial\Omega' \times (0, t)$ . Hence we assume

$$m' \cdot \nu' = 0$$

along  $\partial\Omega'$ . Volume charges, i. e.  $\nabla \cdot m$ , generate a stray field. We assume that

$$\nabla' \cdot m' = \nabla \cdot m \equiv 0.$$

Hence on the mesoscopic level, we arrive at

$$|m'|^2 = 1 \quad \text{and} \quad \nabla' \cdot m' = 0 \quad \text{in } \Omega', \quad m' \cdot \nu' = 0 \quad \text{on } \partial\Omega'. \quad (3)$$

In [7] this mesoscopic thin-film description has been justified by  $\Gamma$ -convergence in the regime of small aspect ratio (i. e.  $t \ll \ell$ , where  $\ell$  is the diameter of the cross-section) and of not too small samples (i. e.  $\ell t \gg d^2 \ln(\ell/t)$ ). We remark that (3) is rather rigid for smooth solutions: This can best be seen by using  $\nabla' \cdot m' = 0$  to write  $m' = \nabla'^{\perp} \psi$  with help of a “stream function”  $\psi$ . Then (3) turns into the Dirichlet problem for the eikonal equation, i. e.

$$|\nabla' \psi|^2 = 1 \quad \text{in } \Omega', \quad \psi = 0 \quad \text{on } \partial\Omega'. \quad (4)$$

It is well-known that (4) does not admit a smooth solution, but many almost-everywhere solutions. One of them is the distance function

$$\psi(x') = \text{dist}(x', \partial\Omega'),$$

which corresponds to the so called Landau state for  $m$ , cf. Figure 2. The distance function generically has ridges; these translate into line singularities on the level of  $m'$ . This is the heuristic explanation why the principle of pole avoidance (i.e. the avoidance of charges) leads to wall formation in thin-film elements.

We notice that the condition  $\nabla' \cdot m' = 0$  in (3), interpreted in the distributional sense, means that the component of  $m'$  normal to the wall does not jump (mesoscopically charge-free walls). This means that (up to rigid motions) a wall is locally determined by a single angle  $\theta$  on this mesoscopic level, which describes the angle between the magnetizations in the adjacent domains, see Figure 3.

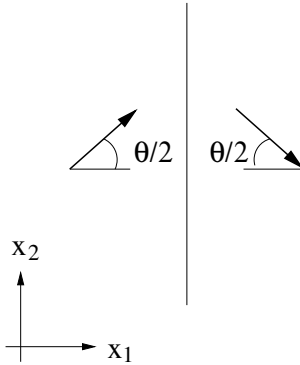


Figure 3: The wall angle

### 1.3 A microscopic view: Different types of walls

The description of walls as discontinuity lines is an idealization of the mesoscopic point of view. On the microscopic level, they are replaced by smooth transition layers. There is a variety of these transition layers; their occurrence depends mainly on the film thickness  $t$ . The most common wall types in thin films are Néel wall, asymmetric Bloch wall and cross-tie wall, which we shall discuss in the sequel.

#### 1.3.1 Néel wall

Out of these three walls the Néel wall has the easiest structure (cf. Fig 4). It is characterized by in-plane and 1-d rotation of the magnetization:

$$m_3 = 0$$

and

$$m = m(x_1).$$

Since then  $\nabla \cdot m = \frac{\partial m_1}{\partial x_1}$ , this necessarily leads to charges. The Néel wall is the dominating wall type in very thin films. Roughly speaking, very thin means that the thickness is small compared to the exchange length:  $t \ll d$ . It is divided in a small core with fast varying rotation and two far-reaching, logarithmically decaying tails (see Figure 5). In infinite samples without anisotropy energy, such a single Néel wall would achieve an arbitrary small energy by spreading over the complete plane. Therefore for the Néel wall to exist, its tails have to be contained. In practice the confining mechanisms are: steric interaction of neighbouring Néel walls, steric interaction with the boundary of the magnetic sample and the anisotropy of the material. This long-range interaction between Néel walls and the boundary of the sample prevents the realisation of global minima of the energy and is thus at the origin of hysteresis effects (cf. [11, p. 242]).

Melcher has given a detailed analysis of the pointwise behaviour of the Néel wall: In [16, 17] pointwise upper and lower bounds with the same logarithmical scaling are proved for the Néel wall tails (the Néel wall in this setting is confined by anisotropy energy rather than by the sample edge).

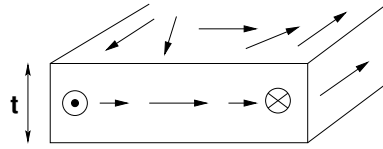


Figure 4: Néel wall

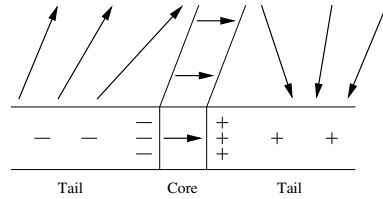


Figure 5: Charge distribution in core and tails of a Néel wall

### 1.3.2 Asymmetric Bloch wall

With increasing film thickness another type of domain wall occurs: The asymmetric Bloch wall. Unlike the Néel wall it is thickness dependent, i.e.

$$m = m(x_1, x_3)$$

but stray field free, i.e.

$$\begin{aligned} \nabla \cdot m &= 0 & \text{in } \Omega' \times (0, t), \\ m_3 &= 0 & \text{on } \Omega' \times \{0, t\}. \end{aligned}$$

This is achieved by a rather complicated pattern (cf. [11, p. 245]). Surprisingly, a model (ansatz) for an exactly stray-field free asymmetric Bloch wall is not so old [10]. The cross-over in the specific wall energy between the asymmetric Bloch wall and the Néel wall has been investigated in [18].

### 1.3.3 Cross-tie wall

In moderately thick films the most common wall type is the cross-tie wall (cf. Figure 6). This is a complicated composite wall where a  $180^\circ$ -Néel wall is replaced by a pattern of Néel wall segments with transition angle of  $90^\circ$  or less. There is a central Néel wall segment along the  $x_1$ -axis, where perpendicular Néel wall segments branch off periodically (lines in mesoscopic view in Figure 6), the so called cross-ties. Topologically this structure enforces the existence of point singularities of the magnetization in the mesoscopic view, the so called Bloch lines. There are circular Bloch lines (white circle) and cross Bloch lines (black circles).

As for the Néel walls the magnetization within the Bloch lines is smooth on a microscopic level. The inner structure of a circular Bloch line (cf. Figure 7) is easy: It is the regularization of a vortex, where the magnetization avoids the singularity by turning out of the plane when approaching the center.

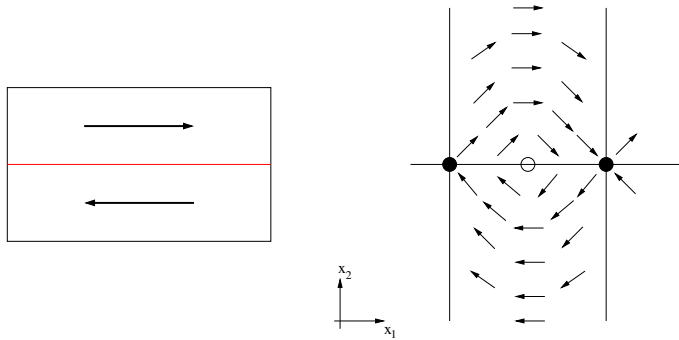


Figure 6: Macroscopic view of cross-tie wall, microscopic pattern

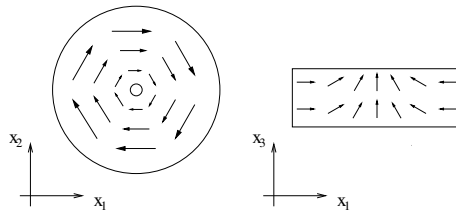


Figure 7: Bloch line (microscopic view)

The reason for this microstructure formation is well understood: The specific line energy of a  $90^\circ$ -Néel wall is only 12% of that of a  $180^\circ$ -Néel wall. While the total wall length in Figure 6 is larger, the total wall energy is smaller than for a single  $180^\circ$ -Néel wall. This overcompensates the energy cost of the Bloch lines.

In fact, an optimal pattern in a thick film regime has been identified in [3]: The authors start from the following expression of an angle-dependent wall energy (which can be justified for moderately thick films):

$$E_{thick}(\theta) = 4dt(\sin(\theta/2) - \theta/2 \cos(\theta/2)). \quad (5)$$

Notice that for small angles,  $E_{thick}(\theta) \sim \theta^3$ . The authors minimize the total wall energy among all magnetizations  $m'$  which satisfy  $|m'|^2 = 1$  and  $\nabla' \cdot m' = 0$  distributionally and connect the constant states  $(-1, 0)$  to  $(1, 0)$  for  $x_2 \uparrow \pm\infty$ . Using a modification of the Null-Lagrangian introduced in [12], they identify a minimizer which is sketched in Figure 6.

The analysis in [3] is oblivious to the length scale of the periodicity of the cross ties. The mechanisms which determine this length scale have been scrutinized in [8]. It is found that the repulsion between the tails of the perpendicular Néel wall segments is the relevant mechanism.

## 1.4 2-d stability of the Néel wall

As explained above, the cross-tie wall occurs because of the strong degeneracy of the specific Néel wall energy in the wall angle  $\theta$ . This degeneracy is even more

pronounced for thin films. The specific line energy can be calculated to behave like

$$E_{thin}(\theta) \approx {}^1 \frac{\pi t^2}{2 \ln \frac{wt}{d^2}} (1 - \cos(\theta/2))^2,$$

where  $w$  is the length to which the Néel wall tails are confined. Notice that for small angles  $E_{thin}(\theta) \sim \theta^4 \ll \theta^3 \sim E_{thick}(\theta)$ . Hence the question arises why cross-tie walls are not observed in thin films. The conjecture is the following: As we have seen the cross-tie wall requires Bloch lines because of topological reasons. In [7] the following scaling of the energy for the Bloch line is heuristically derived:

$$E_{Bloch} \sim d^2 t \ln \frac{\ell}{d}.$$

Since the Néel wall energy tends quadratically to 0 for  $t \downarrow 0$  (cf. Theorem 1), the relative cost of Bloch lines increases with decreasing film thickness. This explains why cross-tie walls are not observed in sufficiently thin films despite the pronounced angle degeneracy.

This does not yet explain why the  $180^\circ$ -Néel wall is stable. This is the question we address in this paper: In view of the above discussion, we suppress Bloch lines and investigate whether arbitrary 2-d (i.e. in-plane) modulations of the 1-d Néel wall may reduce the energy. We find that this is asymptotically not the case.

## 1.5 Related work

There has recently been further research on Modica–Mortola type problems where the homogeneous  $H^1$ -norm is replaced by the homogeneous  $H^{1/2}$ -norm in various fields of applications. One is a model for dislocations in crystals, introduced by Cuitino, Koslowski and Ortiz [14]. In this model, long-range elastic interaction between dislocation lines is represented by a  $H^{1/2}$ -type term. A  $\Gamma$ -limit for this model has been established by Garroni and Müller in [9].

Also in the classical setting of phase separation, the Cahn–Hilliard energy has been extended by an  $H^{1/2}$ -term. This term then describes the effects of line tension at triple junctions. The connection of this generalized Cahn–Hilliard energy and the corresponding geometrical sharp interface model with line tension has been analyzed by Alberti, Bouchitté and Seppecher in [1, 2]. The Gamma-limit for a related energy is derived by Kurzke [15]. The latter energy functional comes from micromagnetism. It describes the behaviour of magnetization in a regime where only exchange energy and surface charge energy survive [13]. The exchange energy is represented as  $H^{1/2}$ -norm on the boundary.

Energies of this type that combine a  $H^1$ -term on the full domain with a potential energy on the boundary are recovered also in a more general analytical setting: The corresponding Euler–Lagrange equations to such energies are the well-known

---

<sup>1</sup>Notation:  $A_\epsilon \approx B_\epsilon$  means  $\lim_{\epsilon \rightarrow 0} A_\epsilon/B_\epsilon = 1$

boundary–reaction equations. The existence of Layer solutions to these equations and their connection to stable solutions has been investigated by Cabré and Solà–Morales in [5].

## 2 Setting and result

The setting is determined by our goal to analyze the stability of Néel walls under 2–d variation. The assumptions on  $m$  are motivated in the previous chapter.

### 2.1 2–d admissible magnetizations

We assume the magnetic sample to have the shape of a thin infinitely extended cylinder:

$$\begin{aligned}\Omega &= \Omega' \times (0, t), \\ \Omega' &= (-w, w) \times \mathbb{R} \subset \mathbb{R}^2.\end{aligned}$$

The finiteness of the sample in  $x_1$ –direction serves as the confining mechanism for the Néel wall tails (cf. Subsection 1.3.1). Since we are interested in thin films, we assume  $m$  to depend only on the tangential variables:

$$m(x) = m(x') \tag{6}$$

and to be in–plane

$$m_3(x) = 0. \tag{7}$$

We enforce a mesoscopic 180°–transition angle by imposing

$$m'(x) = \begin{pmatrix} 0 \\ \pm 1 \end{pmatrix} \quad \text{for } x_1 = \pm w. \tag{8}$$

The infinite  $x_2$ –direction excludes boundary effects in the tangential direction. In order to be able to assign an energy density to our configuration we assume that  $m$  is periodic in the infinite  $x_2$ –direction:

$$m(x_1, x_2 + \ell) = m(x_1, x_2). \tag{9}$$

The period  $\ell$  can be chosen arbitrarily large; our estimates do not depend on this constant. In this setting, a wall is one–dimensional if  $m = m(x_1)$ .

We expect the Euler–Lagrange equations to enforce regularity of the minimizers. We therefore explicitly request:

$$m \text{ is continuously differentiable in } [-w, w] \times \mathbb{R}. \tag{10}$$

## 2.2 2-d thin film energy

We use a thin-film approximation to  $E_{3d}$ , which shall be heuristically motivated in this section: We first write the stray field equation (2) as follows:

$$\Delta\left(\frac{1}{t}u\right) = \left(\frac{1}{t}\chi_{(0,t)}\right)\nabla' \cdot m'. \quad (11)$$

The right hand side of (11) converges for  $t \rightarrow 0$  to a distribution supported on  $\{x_3 = 0\}$ . Hence we expect  $u/t$  to converge to the solution  $U$  of

$$\Delta U = \nabla' \cdot m' \mathcal{H}^2[\{x_3 = 0\}]. \quad (12)$$

Using this approximate stray field we arrive at the following expression for the energy:

$$\ell E_{2d}(m') := d^2t \int_{(-w,w) \times [0,\ell]} |\nabla' m'|^2 dx' + t^2 \int_{\mathbb{R}^2 \times [0,\ell]} |\nabla U|^2 dx,$$

(cf. [7]). We now non-dimensionalize our problem. We measure length with respect to the transversal size:

$$x = w\hat{x} \quad \text{and} \quad \ell = w\hat{\ell}$$

and rescale energy by

$$E_{2d} = t^2 \hat{E}_{2d}.$$

Then we obtain the following expression for the energy:

$$\hat{\ell} \hat{E}_{2d}(m') := \epsilon \int_{(-1,1) \times [0,\hat{\ell}]} |\hat{\nabla}' m'|^2 d\hat{x}' + \int_{\mathbb{R}^2 \times [0,\hat{\ell}]} |\hat{\nabla} U|^2 d\hat{x},$$

where the dimensionless parameter  $\epsilon \ll 1$  is defined by

$$\epsilon := \frac{d^2}{tw}.$$

In the sequel we will drop the hats.

## 2.3 Fourier representation

From now on we think of the magnetization as being constantly extended outside the magnetic sample, i.e.

$$m'(x) = \begin{pmatrix} 0 \\ \pm 1 \end{pmatrix} \quad \text{for } \pm x_1 \geq w. \quad (13)$$

This does not affect the energy. The stray field equation (12) can be solved explicitly in Fourier space. We first introduce our notation of Fourier transformation: Given a function  $\phi(x)$  which is  $\ell$ -periodic in  $x_2$ , we introduce the combination of Fourier transformation in  $x_1$  and Fourier series in  $x_2$  by

$$\mathcal{F}\phi(k) = \frac{1}{\sqrt{2\pi\ell}} \int_{\mathbb{R} \times [0,\ell)} e^{ik \cdot x} \phi(x) dx \quad \text{where } k \in \mathbb{R} \times \frac{2\pi}{\ell} \mathbb{Z}.$$

We also introduce the notation

$$\int_{\mathbb{R} \times \frac{2\pi}{\ell} \mathbb{Z}} \cdot dk = \sum_{k_2 \in \frac{2\pi}{\ell} \mathbb{Z}} \int_{\mathbb{R}} \cdot dk_1.$$

With this notation we have

$$\begin{aligned} \int_{\mathbb{R} \times [0,\ell)} \phi \bar{\sigma} dx &= \int_{\mathbb{R} \times \frac{2\pi}{\ell} \mathbb{Z}} \mathcal{F}\phi \overline{\mathcal{F}\sigma} dk, \\ \int_{\mathbb{R} \times [0,\ell)} |\nabla^\alpha \phi|^2 dx &= \int_{\mathbb{R} \times \frac{2\pi}{\ell} \mathbb{Z}} |k|^{2\alpha} |\mathcal{F}\phi|^2 dk. \end{aligned}$$

Solving the stray field equation (12) we obtain the representation of the energy used in this paper:

$$\ell E_{2d}(m') = \epsilon \int_{\mathbb{R} \times [0,\ell)} |\nabla' m'|^2 dx' + \frac{1}{2} \int_{\mathbb{R} \times [0,\ell)} |\nabla'^{-1/2} \nabla' \cdot m'|^2 dx'.$$

In fact this energy is a good approximation of  $E_{3d}$  in the thin film regime  $t \ll d$ .

In the sequel we will drop the primes.

## 2.4 Statement of the result

Our main result shows that asymptotically, the minimal energy is assumed by a 1-d transition layer. More precisely, variations of the optimal 1-d transition layer in  $x_2$ -direction cannot decrease the leading order coefficient of the energy.

Let us recall our setting in non-dimensionalized variables: Admissible functions  $m: \mathbb{R}^2 \rightarrow \mathbb{R}^2$  are continuously differentiable and satisfy

$$|m|^2 = 1, \tag{14}$$

$$m = \begin{pmatrix} 0 \\ \pm 1 \end{pmatrix} \quad \text{for } \pm x_1 \geq 1, \tag{15}$$

$$m(x_1, x_2 + \ell) = m(x_1, x_2) \quad \text{for all } x = (x_1, x_2) \in \mathbb{R}^2. \tag{16}$$

The energy is given by

$$\ell E_{2d}(m) = \epsilon \int_{\mathbb{R} \times [0,\ell)} |\nabla m|^2 dx + \frac{1}{2} \int_{\mathbb{R} \times [0,\ell)} |\nabla^{-1/2} \nabla \cdot m|^2 dx.$$

Our main result is

**Theorem 1.** *For  $\epsilon \ll 1$  we have*

$$\min_{m \text{ satisfies } (14),(15),(16)} E_{2d}(m) \approx \min_{m \text{ satisfies } (14),(15),(16), m=m(x_1)} E_{2d}(m) \approx \frac{\pi}{2 \ln \frac{1}{\epsilon}}.$$

The theorem is an immediate consequence of the following two propositions.

**Proposition 1.** *For  $\epsilon \ll 1$  there exists a smooth  $m$  satisfying (14), (15) & (16) and  $m = m(x_1)$  such that*

$$E_{2d}(m) \lesssim \frac{\pi}{2 \ln \frac{1}{\epsilon}}.$$

**Proposition 2.** *For  $\epsilon \ll 1$  and any  $\ell$  and smooth  $m$  satisfying (14), (15) & (16) we have*

$$E_{2d}(m) \gtrsim \frac{\pi}{2 \ln \frac{1}{\epsilon}}.$$

In dimensional variables the theorem can be stated as follows: For

$$\frac{d^2}{t} \ll w \tag{17}$$

we have

$$\min_m E_{2d}(m) \approx \min_{m \text{ satisfies } m=m(x_1)} E_{2d}(m) \approx \frac{\pi t^2}{2 \ln \frac{wt}{d^2}}.$$

The regime (17) can be understood as follows: The Néel wall core scales like  $d^2/t$  (cf. [8, p. 15]). Our regime therefore just assures that the typical Néel wall structure consists of core and tails has a chance to exist in the sample of size  $2w$ .

## 3 Proofs

### 3.1 Proof of Proposition 1

The additional assumption  $m = m(x_1)$  allows us to further simplify the 2-d energy to:

$$E_{1d}(m) = \epsilon \int_{\mathbb{R}} \left| \frac{d}{dx_1} m \right|^2 dx_1 + \frac{1}{2} \int_{\mathbb{R}} \left| \left( \frac{d}{dx_1} \right)^{1/2} m_1 \right|^2 dx_1.$$

The proof of the 1-d upper (and lower) bound is well-known, we refer to [6, 17, 8]. For the convenience of the reader, we will reproduce the proof and make a few philosophical remarks.

We will construct an  $m_1 \in C^0(\mathbb{R}) \cap H^1(\mathbb{R})$  with the following properties

$$m_1 \left\{ \begin{array}{lll} = & 1 & \text{at } x_1 = 0, \\ \in & (0, 1) & \text{on } (-1, 1), \\ = & 0 & \text{on } \mathbb{R} - [-1, 1] \end{array} \right\}. \tag{18}$$

We then set

$$m_2(x_1) = \left\{ \begin{array}{ll} \sqrt{1 - m_1(x_1)^2} & \text{for } x_1 \geq 0, \\ -\sqrt{1 - m_1(x_1)^2} & \text{for } x_1 \leq 0 \end{array} \right\}.$$

Then  $m = (m_1, m_2)$  satisfies (14) & (15) by construction.

Our construction is based on the fact there does *not* exist an estimate of the form

$$\sup_{\mathbb{R}} |m_1|^2 \leq C \int_{\mathbb{R}} \left| \left( \frac{d}{dx_1} \right)^{1/2} m_1 \right|^2 dx_1, \quad (19)$$

despite the fact that both sides have the same scaling in  $x_1$  and  $m_1$ . In fact, if (19) were true, there would be an estimate

$$\sup_{\mathbb{R}^2} |\bar{m}_1|^2 \leq \frac{C}{2} \int_{\mathbb{R}^2} |\nabla \bar{m}_1|^2 dx_1 dx_3. \quad (20)$$

This would follow from the trace characterization of the homogeneous  $H^{1/2}$ -norm:

$$\int_{\mathbb{R}} \left| \left( \frac{d}{dx_1} \right)^{1/2} m_1 \right|^2 dx_1 = \inf \left\{ \frac{1}{2} \int_{\mathbb{R}^2} |\nabla \bar{m}_1|^2 dx_1 dx_3 \mid \bar{m}(x_1, 0) = m(x_1) \right\}. \quad (21)$$

Finally, if (20) were true, there would be an estimate of the form

$$\int_{\mathbb{R}^2} |\nabla \bar{m}_1|^2 dx_1 dx_3 \leq \frac{C}{2} \left( \int_{\mathbb{R}^2} |\Delta \bar{m}_1| dx_1 dx_3 \right)^2. \quad (22)$$

This would follow from the integration by parts:

$$\int_{\mathbb{R}^2} |\bar{\nabla} m_1|^2 dx_1 dx_3 = \int_{\mathbb{R}^2} (-\Delta \bar{m}_1) \bar{m}_1 dx_1 dx_3.$$

The counter example for (22) is based on the observation that the logarithmic Green's function

$$\bar{m}_1(x_1, x_3) = \frac{1}{2\pi} \ln \frac{1}{r} \quad \text{where } r = \sqrt{x_1^2 + x_3^2} \quad (23)$$

formally satisfies

$$\begin{aligned} \int_{\mathbb{R}^2} |\Delta \bar{m}_1| dx_1 dx_3 &= 1 \quad \text{but} \\ \int_{\mathbb{R}^2} |\nabla \bar{m}_1|^2 dx_1 dx_3 &= \frac{1}{2\pi} \int_0^\infty \frac{1}{r} dr = +\infty. \end{aligned}$$

In order to turn (23) into a proper counterexample to (22), we cut off the infinity at  $r = 0$  and the infinity at  $r = \infty$ :

$$\bar{m}_{1,\epsilon}(x_1, x_3) = \begin{cases} \frac{\ln \frac{1}{\sqrt{r^2 + \epsilon^2}}}{\ln \frac{1}{\epsilon}} & \text{for } r \leq \sqrt{1 - \epsilon^2}, \\ 0 & \text{else} \end{cases}.$$

Notice that  $\bar{m}_{1,\epsilon}$  is normalized such that

$$\sup_{\mathbb{R}^2} |\bar{m}_{1,\epsilon}|^2 = 1$$

and satisfies

$$\int_{\mathbb{R}^2} |\nabla \bar{m}_{1,\epsilon}|^2 dx = \frac{2\pi}{\ln^2 \frac{1}{\epsilon}} \int_0^{\sqrt{1-\epsilon^2}} \frac{r^3}{(r^2 + \epsilon^2)^2} dr \approx \frac{2\pi}{\ln \frac{1}{\epsilon}}.$$

Therefore,  $\{\bar{m}_{1,\epsilon}\}_{\epsilon \downarrow 0}$  shows that (20) cannot be true.

At the same time,  $\bar{m}_{1,\epsilon}$  yields the desired construction for the upper bound. Indeed, consider

$$m_{1,\epsilon}(x_1) = \bar{m}_{1,\delta}(x_1, 0),$$

where  $\delta := \epsilon \ln \frac{1}{\epsilon}$  is chosen such that in the regime  $\epsilon \ll 1$

$$\ln \frac{1}{\delta} \approx \ln \frac{1}{\epsilon}$$

both variables have the same logarithmic behaviour. It obviously satisfies (18). In view of (21), we have

$$\frac{1}{2} \int_{\mathbb{R}} \left| \left( \frac{d}{dx_1} \right)^{1/2} m_{1,\delta} \right|^2 dx_1 \leq \frac{1}{4} \int_{\mathbb{R}^2} |\nabla \bar{m}_{1,\delta}|^2 dx \approx \frac{\pi}{2 \ln \frac{1}{\epsilon}}.$$

It remains to argue that the exchange energy is of lower order: With help of (14) we reduce the statement to a statement on  $m_1$  by:

$$|\nabla m_\delta|^2 \leq \frac{\left| \frac{d}{dx_1} m_{1,\delta} \right|^2}{1 - m_{1,\delta}}.$$

Using this identity one easily computes:

$$\begin{aligned} \epsilon \int_{\mathbb{R}} |\nabla m_\delta|^2 dx &\leq \frac{2\epsilon}{\ln \frac{1}{\delta}} \int_{\mathbb{R}} \frac{x_1^2}{(x_1^2 + \delta^2)^2 \ln \frac{\delta^2}{x_1^2 + \delta^2}} dx \\ &\lesssim \frac{\epsilon}{\delta \ln \frac{1}{\delta}} \\ &\approx \frac{1}{\ln^2 \frac{1}{\epsilon}}. \end{aligned}$$

This shows that the exchange part of the energy is of lower order. To conclude the proof it remains to approximate  $m_{1,\delta}$  in  $H^1(\mathbb{R})$  by smooth functions.  $\square$

### 3.2 Proof of Proposition 2

We start by identifying a (curved) center line of the transition layer. It is given by the boundary  $\partial G$  (with outer normal  $\nu$ ) of a set  $G \subset \mathbb{R}^2$  with the following properties

$$G \quad \text{is } \ell\text{-periodic in } x_2, \tag{24}$$

$$m = \nu \quad \text{on } \partial G. \tag{25}$$

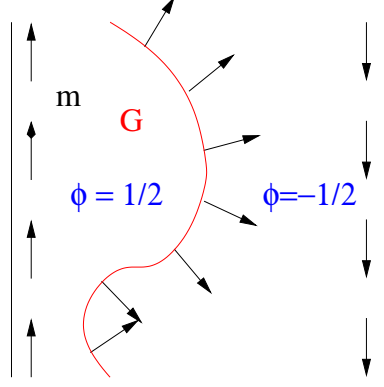


Figure 8: Center line of the wall

The existence of such a set follows from a dynamical systems argument: Consider the rotated magnetization  $m^\perp = (-m_2, m_1)$ . According to (16), it can be regarded as a vector field on  $\mathbb{R} \times S^1$ . According to (15),  $m^\perp$  points inwards on  $(\mathbb{R} - (-1, 1)) \times S^1$ . According to (14), it does not have a stationary point. Hence by the Poincaré–Bendixson theorem [20, Theorem 4.5],  $m^\perp$  must admit a closed orbit in  $(-1, 1) \times S^1$ , which separates  $\mathbb{R} \times S^1$  into a left and a right part. Call the left part  $G$ , then  $m^\perp$  is tangential along  $\partial G$ . In view of (16) this means that  $m$  agrees with the outer normal  $\nu$  of  $\partial G$ .

We will actually prove the following stronger version of Proposition 2:

$$\ell \min E_{2d}(m) \gtrsim \frac{\pi}{2 \ln \frac{1}{\epsilon}} \text{length}(\partial G \cap (\mathbb{R} \times [0, \ell))). \quad (26)$$

Notice that (26) is indeed a stronger version since due to (24)

$$\text{length}(\partial G \cap (\mathbb{R} \times [0, \ell))) \geq \ell.$$

Our lower bound is based on a dual argument passing via the divergence  $\sigma = \nabla \cdot m$ . We note that  $G$  is just constructed such that

$$\int_{G \cap (\mathbb{R} \times [0, \ell))} \sigma \, dx \stackrel{(15), (16), (24)}{=} \int_{\partial G \cap (\mathbb{R} \times [0, \ell))} m \cdot \nu \, ds \stackrel{(25)}{=} \text{length}(\partial G \cap (\mathbb{R} \times [0, \ell))). \quad (27)$$

We rephrase (27) in terms of the “test function”

$$\phi = \left\{ \begin{array}{ll} \frac{1}{2} & \text{on } G \\ -\frac{1}{2} & \text{on } \mathbb{R}^2 - G \end{array} \right\} \quad (28)$$

as

$$\int_{\mathbb{R} \times [0, \ell)} \phi \sigma \, dx = \text{length}(\partial G \cap (\mathbb{R} \times [0, \ell))). \quad (29)$$

We remark for further reference

$$\int_{\mathbb{R} \times [0, \ell)} |\nabla \phi| \, dx = \text{length}(\partial G \cap (\mathbb{R} \times [0, \ell))) \quad \text{and} \quad \sup_{\mathbb{R} \times [0, \ell)} |\phi| = \frac{1}{2}, \quad (30)$$

where  $\int |\nabla\phi| dx$  is to be interpreted in the  $BV$ -sense.

On the other hand it follows from

$$|\nabla \cdot m|^2 \leq 2 |\nabla m|^2$$

that

$$\frac{\epsilon}{2} \int_{\mathbb{R} \times [0, \ell]} |\sigma|^2 dx + \frac{1}{2} \int_{\mathbb{R} \times [0, \ell]} |\nabla^{-1/2} \sigma|^2 dx \leq \ell E_{2d}(m). \quad (31)$$

For further reference we remark that

$$\int_{\mathbb{R} \times [0, \ell]} |\nabla^{-1} \sigma|^2 dx \leq 2 \ell. \quad (32)$$

Indeed, let  $\zeta(x_1, x_2)$  a smooth function which is  $\ell$ -periodic in  $x_2$  and decaying in  $x_1$ . Then we have

$$\begin{aligned} \int_{\mathbb{R} \times [0, \ell]} \sigma \zeta dx &= - \int_{\mathbb{R} \times [0, \ell]} m \cdot \nabla \zeta dx \\ &\stackrel{(15)}{=} - \int_{(-1, 1) \times [0, \ell]} m \cdot \nabla \zeta dx \\ &\stackrel{(14)}{\leq} \left( 2 \ell \int_{\mathbb{R} \times [0, \ell]} |\nabla \zeta|^2 dx \right)^{1/2}, \end{aligned}$$

which implies (32) by duality.

The duality argument is based on the fact that the estimate

$$\int_{\mathbb{R} \times [0, \ell]} |\nabla^{1/2} \phi|^2 dx \leq C \sup_{\mathbb{R} \times [0, \ell]} |\phi| \int_{\mathbb{R} \times [0, \ell]} |\nabla \phi| dx \quad (33)$$

is almost true, i. e. that it just fails logarithmically. Indeed both sides of (33) have the same scaling in  $x$  and  $\phi$ . We now argue why it fails: Recall that

$$\int_{\mathbb{R} \times [0, \ell]} |\nabla^{1/2} \phi|^2 dx = \int_{\mathbb{R} \times \frac{2\pi}{\ell} \mathbb{Z}} |k| |\mathcal{F}\phi|^2 dk \quad (34)$$

Notice that for  $\phi$  of the form (28) with  $G = (-\infty, 0) \times \mathbb{R}$  the half space, i. e.

$$\phi(x_1, x_2) = \left\{ \begin{array}{ll} \frac{1}{2} & \text{for } x_1 < 0, \\ -\frac{1}{2} & \text{for } x_1 > 0 \end{array} \right\} \quad (35)$$

we have

$$(\mathcal{F}\phi)(k_1, k_2) = \left\{ \begin{array}{ll} -\sqrt{\frac{\ell}{2\pi}} \frac{i}{k_1} & \text{for } k_2 = 0, \\ 0 & \text{else} \end{array} \right\}.$$

Hence (34) diverges logarithmically, i. e.

$$\int_{\mathbb{R} \times \frac{2\pi}{\ell} \mathbb{Z}} |k| |\mathcal{F}\phi|^2 dk = \frac{\ell}{\pi} \int_0^\infty \frac{1}{k_1} dk_1 = +\infty, \quad (36)$$

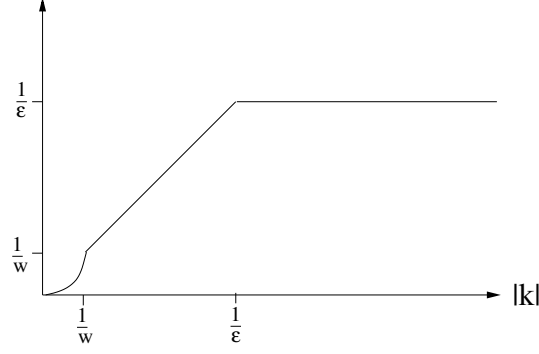


Figure 9: Regularized  $H^{1/2}(\mathbb{R})$ -multiplier

whereas the right hand side of (33) is finite, i. e.

$$\sup_{\mathbb{R} \times [0, \ell)} |\phi| \int_{\mathbb{R} \times [0, \ell)} |\nabla \phi| dx = \frac{1}{2} \ell. \quad (37)$$

We also notice that the 1-d estimate (19) would be a consequence of (33) (in its 1-d version) by duality. Indeed, this follows from

$$m_1(0)^2 = \left( \int_{\mathbb{R}} \frac{dm_1}{dx_1} \phi dx_1 \right)^2 \leq \int_{\mathbb{R}} \left| \left( \frac{d}{dx_1} \right)^{1/2} m_1 \right|^2 dx_1 \int_{\mathbb{R}} \left| \left( \frac{d}{dx_1} \right)^{1/2} \phi \right|^2 dx_1$$

for the  $\phi$  defined in (35).

An estimate of the form (33) holds provided one cuts off the very small ( $\leq \epsilon$ ) and the very large scales ( $\geq w$ ). The constant depends logarithmically on the ratio  $\frac{w}{\epsilon}$  of large scale cut-off and small scale cut-off. The following lemma identifies the optimal prefactor  $\frac{2}{\pi}$ . The optimality of the prefactor can be seen from comparing (36) and (37).

**Lemma 1.** *For  $\epsilon \ll w$  and any  $\phi$  which is  $\ell$ -periodic in  $x_2$  we have*

$$\int_{\mathbb{R} \times \frac{2\pi}{\ell} \mathbb{Z}} \min\left\{ \frac{1}{\epsilon}, |k|, w|k|^2 \right\} |\mathcal{F}\phi|^2 dk \lesssim \frac{2}{\pi} \left( \ln \frac{w}{\epsilon} \right) \sup_{\mathbb{R} \times [0, \ell)} |\phi| \int_{\mathbb{R} \times [0, \ell)} |\nabla \phi| dx. \quad (38)$$

PROOF OF PROPOSITION 2, CONTINUED.

Before we prove Lemma 1, let us finish the proof of the proposition. We have

$$\begin{aligned}
& \text{length}(\partial G \cap (\mathbb{R} \times [0, \ell])) \\
& \stackrel{(29)}{=} \int_{\mathbb{R} \times [0, \ell]} \phi \sigma \, dx \\
& = \int_{\mathbb{R} \times \frac{2\pi}{\ell} \mathbb{Z}} \mathcal{F}\phi \overline{\mathcal{F}\sigma} \, dk \\
& \leq \left( \int_{\mathbb{R} \times \frac{2\pi}{\ell} \mathbb{Z}} \left( \frac{\epsilon}{2} + \frac{1}{2|k|} + \frac{1}{2w|k|^2} \right)^{-1} |\mathcal{F}\phi|^2 \, dk \right)^{1/2} \\
& \quad \times \left( \int_{\mathbb{R} \times \frac{2\pi}{\ell} \mathbb{Z}} \left( \frac{\epsilon}{2} + \frac{1}{2|k|} + \frac{1}{2w|k|^2} \right) |\mathcal{F}\sigma|^2 \, dk \right)^{1/2} \\
& \leq \left( \int_{\mathbb{R} \times \frac{2\pi}{\ell} \mathbb{Z}} 2 \min\left\{ \frac{1}{\epsilon}, |k|, w|k|^2 \right\} |\mathcal{F}\phi|^2 \, dk \right)^{1/2} \\
& \quad \times \left( \int_{\mathbb{R} \times \frac{2\pi}{\ell} \mathbb{Z}} \left( \frac{\epsilon}{2} + \frac{1}{2|k|} + \frac{1}{2w|k|^2} \right) |\mathcal{F}\sigma|^2 \, dk \right)^{1/2} \\
& \stackrel{(38)}{\lesssim} \left( \frac{4}{\pi} \left( \ln \frac{w}{\epsilon} \right) \sup_{\mathbb{R} \times [0, \ell]} |\phi| \int_{\mathbb{R} \times [0, \ell]} |\nabla \phi| \, dx \right)^{1/2} \\
& \quad \times \left( \frac{\epsilon}{2} \int_{\mathbb{R} \times [0, \ell]} |\sigma|^2 \, dx + \frac{1}{2} \int_{\mathbb{R} \times [0, \ell]} |\nabla^{-1/2} \sigma|^2 \, dx + \frac{1}{2w} \int_{\mathbb{R} \times [0, \ell]} |\nabla^{-1} \sigma|^2 \, dx \right)^{1/2} \\
& \stackrel{(30), (31), (32)}{\leq} \left( \frac{4}{\pi} \left( \ln \frac{w}{\epsilon} \right) \frac{1}{2} \text{length}(\partial G \cap (\mathbb{R} \times [0, \ell])) \right)^{1/2} \left( \ell (E_{2d}(m) + \frac{1}{w}) \right)^{1/2}.
\end{aligned}$$

This yields

$$\ell (E_{2d}(m) + \frac{1}{w}) \gtrsim \frac{\pi}{2 \ln \frac{w}{\epsilon}} \text{length}(\partial G \cap (\mathbb{R} \times [0, \ell])).$$

It remains to select a  $w = w(\epsilon)$  such that

$$\ln \frac{1}{\epsilon} \ll w \quad \text{and} \quad \ln w \ll \ln \frac{1}{\epsilon}.$$

PROOF OF LEMMA 1.

The first step is to establish the identity

$$\int_{\mathbb{R}^2} |1 - e^{iz_1}|^2 \frac{1}{|z|^3} \, dz = 4\pi. \tag{39}$$

This can be seen in polar coordinates:

$$\begin{aligned}
\int_{\mathbb{R}^2} |1 - e^{iz_1}|^2 \frac{1}{|z|^3} dz &= 4 \int_0^{2\pi} \int_0^\infty \sin^2\left(\frac{r \cos \theta}{2}\right) \frac{1}{r^2} d\theta dr \\
&= 2 \int_0^{2\pi} |\cos \theta| d\theta \int_0^\infty \frac{\sin^2 \rho}{\rho^2} d\rho \\
&= 2 \cdot 4 \cdot \frac{\pi}{2} \\
&= 4\pi,
\end{aligned}$$

(cf. [4, 21.6.1. (21.8)]).

In the second step we perturb (39) to obtain an estimate of the Fourier multiplier. More precisely, we show that for  $\epsilon \leq w$  and  $M \gg 1$

$$\min\left\{\frac{1}{\epsilon}, |k|, w|k|^2\right\} \lesssim \frac{1}{4\pi} \int_{B_{Mw} - B_{M^{-1}\epsilon}} |1 - e^{ik \cdot z}|^2 \frac{1}{|z|^3} dz. \quad (40)$$

Indeed, by scaling and rotational invariance we have

$$\int_{B_{Mw} - B_{M^{-1}\epsilon}} |1 - e^{ik \cdot z}|^2 \frac{1}{|z|^3} dz = |k| \int_{B_{Mw|k|} - B_{M^{-1}\epsilon|k|}} |1 - e^{iz_1}|^2 \frac{1}{|z|^3} dz,$$

so that (40) can be reduced to the case of  $k = (1, 0)$ :

$$\min\left\{\frac{1}{\epsilon}, 1, w\right\} \lesssim \frac{1}{4\pi} \int_{B_{Mw} - B_{M^{-1}\epsilon}} |1 - e^{iz_1}|^2 \frac{1}{|z|^3} dz. \quad (41)$$

We distinguish the cases

$$\begin{array}{ccccc}
M^{-1/2}\epsilon & \leq & 1 & \leq & M^{1/2}w, \\
M^{-1/2}\epsilon & \leq & M^{1/2}w & \leq & 1, \\
1 & \leq & M^{-1/2}\epsilon & \leq & M^{1/2}w.
\end{array}$$

For  $M^{-1/2}\epsilon \leq 1 \leq M^{1/2}w$  we have thanks to  $M \gg 1$  that  $M^{-1}\epsilon \ll 1 \ll Mw$  so that

$$\int_{B_{Mw} - B_{M^{-1}\epsilon}} |1 - e^{iz_1}|^2 \frac{1}{|z|^3} dz \approx \int_{\mathbb{R}^2} |1 - e^{iz_1}|^2 \frac{1}{|z|^3} dz \stackrel{(39)}{=} 4\pi.$$

For  $M^{-1/2}\epsilon \leq M^{1/2}w \leq 1$  we have

$$\begin{aligned}
\int_{B_{Mw} - B_{M^{-1}\epsilon}} |1 - e^{iz_1}|^2 \frac{1}{|z|^3} dz &\geq \int_{B_{M^{1/2}w} - B_{M^{-1}\epsilon}} |1 - e^{iz_1}|^2 \frac{1}{|z|^3} dz \\
&\stackrel{M^{1/2}w \leq 1}{\sim} \int_{B_{M^{1/2}w} - B_{M^{-1}\epsilon}} z_1^2 \frac{1}{|z|^3} dz \\
&\sim M^{1/2}w - M^{-1}\epsilon \\
&\stackrel{M^{-1}\epsilon \ll M^{1/2}w}{\approx} M^{1/2}w \stackrel{M \gg 1}{\gg} w,
\end{aligned}$$

so that in particular

$$\int_{B_{Mw}-B_{M^{-1}\epsilon}} |1 - e^{iz_1}|^2 \frac{1}{|z|^3} dz \geq 4\pi w.$$

Finally, for  $1 \leq M^{-1/2}\epsilon \leq M^{1/2}w$  we have

$$\begin{aligned} \int_{B_{Mw}-B_{M^{-1}\epsilon}} |1 - e^{iz_1}|^2 \frac{1}{|z|^3} dz &\geq \int_{B_{Mw}-B_{M^{-1/2}\epsilon}} |1 - e^{iz_1}|^2 \frac{1}{|z|^3} dz \\ &\stackrel{M^{-1/2}\epsilon \geq 1}{\sim} \int_{B_{Mw}-B_{M^{-1/2}\epsilon}} \frac{1}{|z|^3} dz \\ &\sim \frac{M^{1/2}}{\epsilon} - \frac{1}{Mw} \\ &\stackrel{M^{-1/2}\epsilon \ll Mw}{\approx} \frac{M^{1/2}}{\epsilon} \stackrel{M \gg 1}{\gg} \frac{1}{\epsilon}. \end{aligned}$$

This establishes (41).

Using (40) and changing the order of integration, we may pass from the Fourier side to the real space side:

$$\begin{aligned} &\int_{\mathbb{R} \times \frac{2\pi}{\ell}\mathbb{Z}} \min\left\{\frac{1}{\epsilon}, |k|, w|k|^2\right\} |\mathcal{F}\phi|^2 dk \\ &\quad \lesssim \frac{1}{4\pi} \int_{B_{Mw}-B_{M^{-1}\epsilon}} \int_{\mathbb{R} \times \frac{2\pi}{\ell}\mathbb{Z}} |1 - e^{ik \cdot z}|^2 |\mathcal{F}\phi|^2 dk \frac{1}{|z|^3} dz \\ &= \frac{1}{4\pi} \int_{B_{Mw}-B_{M^{-1}\epsilon}} \int_{\mathbb{R} \times [0, \ell]} |\phi(x) - \phi(x+z)|^2 dx \frac{1}{|z|^3} dz. \end{aligned} \quad (42)$$

We estimate the inner integral rather conventionally:

$$\begin{aligned} &\int_{\mathbb{R} \times [0, \ell]} |\phi(x) - \phi(x+z)|^2 dx \\ &\leq \sup_{x \in \mathbb{R} \times [0, \ell]} |\phi(x) - \phi(x+z)| \int_{\mathbb{R} \times [0, \ell]} |\phi(x) - \phi(x+z)| dx \\ &\leq 2 \sup_{\mathbb{R} \times [0, \ell]} |\phi| \int_{\mathbb{R} \times [0, \ell]} |\nabla\phi \cdot z| dx. \end{aligned} \quad (43)$$

Inserting (43) into (42) and changing again the order of integration we obtain

$$\begin{aligned} &\int_{\mathbb{R} \times \frac{2\pi}{\ell}\mathbb{Z}} \min\left\{\frac{1}{\epsilon}, |k|, w|k|^2\right\} |\mathcal{F}\phi|^2 dk \\ &\quad \lesssim \frac{1}{2\pi} \sup_{\mathbb{R} \times [0, \ell]} |\phi| \int_{\mathbb{R} \times [0, \ell]} \int_{B_{Mw}-B_{M^{-1}\epsilon}} |\nabla\phi(x) \cdot z| \frac{1}{|z|^3} dz dx. \end{aligned} \quad (44)$$

The inner integral is easily computed:

$$\int_{B_{Mw}-B_{M^{-1}\epsilon}} |\nabla\phi(x) \cdot z| \frac{1}{|z|^3} dz = 4 \left(\ln \frac{Mw}{M^{-1}\epsilon}\right) |\nabla\phi(x)|. \quad (45)$$

Inserting (45) into (44) yields

$$\begin{aligned} & \int_{\mathbb{R} \times \frac{2\pi}{\ell} \mathbb{Z}} \min\left\{\frac{1}{\epsilon}, |k|, w|k|^2\right\} |\mathcal{F}\phi|^2 dk \\ & \lesssim \frac{2}{\pi} \left(\ln \frac{Mw}{M^{-1}\epsilon}\right) \sup_{\mathbb{R} \times [0, \ell)} |\phi| \int_{\mathbb{R} \times [0, \ell)} |\nabla\phi| dx. \end{aligned}$$

This is a short version for the following statement: For any  $\delta > 0$  and  $\epsilon \leq w$  there exists  $M_\delta \gg 1$  such that

$$\begin{aligned} & \int_{\mathbb{R} \times \frac{2\pi}{\ell} \mathbb{Z}} \min\left\{\frac{1}{\epsilon}, |k|, w|k|^2\right\} |\mathcal{F}\phi|^2 dk \\ & \leq (1 + \delta) \frac{2}{\pi} \left(\ln \frac{w}{\epsilon} + 2 \ln M_\delta\right) \sup_{\mathbb{R} \times [0, \ell)} |\phi| \int_{\mathbb{R} \times [0, \ell)} |\nabla\phi| dx. \end{aligned}$$

Hence we have to consider  $\epsilon \ll w$  so that  $2 \ln M_\delta \leq \delta \ln \frac{w}{\epsilon}$ . □

## 4 Acknowledgements

HK and FO acknowledge support by the Deutsche Forschungsgemeinschaft through SFB 611 ‘‘Singular phenomena and scaling in mathematical models’’ at the University of Bonn.

## References

- [1] Alberti, G., Bouchitté, G., Seppecher, P., Un résultat de perturbations singulières avec la norme  $H^{1/2}$ . *C. R. Acad. Sci. Paris Sér. I Math.*, **319**(4) (1994), pp. 333–338.
- [2] Alberti, G., Bouchitté, G., Seppecher, P., Phase transition with the line-tension effect. *Arch. Rational Mech. Anal.*, **144**(1) (1998), pp. 1–46.
- [3] Alouges, F., Rivière, T., Serfaty, S., Néel and cross-tie wall energies for planar micromagnetic configurations. *ESAIM Control Optim. Calc. Var.*, **8** (2002), pp. 31–68 (electronic). A tribute to J. L. Lions.
- [4] Bronstein, Semendjajew, Musiol, Mühlig, *Taschenbuch der Mathematik*. Verlag Harri Deutsch.
- [5] Cabré, Solà-Morales, Layer solutions in a halfspace for boundary reactions. *to appear*.
- [6] Cervera, G., *Magnetic domains and magnetic domain walls*. PhD thesis, New York University, 1999.

- [7] Desimone, A., Kohn, R. V., Müller, S., Otto, F., A reduced theory for thin-film micromagnetics. *Comm. Pure Appl. Math.*, **55(11)** (2002), pp. 1408–1460.
- [8] Desimone, A., Kohn, R. V., Müller, S., Otto, F., Repulsive interaction of Néel walls, and the internal length scale of the cross-tie wall. *Multiscale Model. Simul.*, **1(1)** (2003), pp. 57–104 (electronic).
- [9] Garroni, A., Müller, S.,  $\Gamma$ -limit of a phase-field model of dislocations. *SIAM J. Math. Anal.*, **36(6)** (2005), pp. 1943–1964 (electronic).
- [10] Holz, A., Hubert, A. *Phys. Stat. Sol. (B)*, **46** (1971), pp. 377–384.
- [11] Hubert, A., Schäfer, R., *Magnetic domains: The analysis of magnetic microstructures*. Springer–Verlag, 1998.
- [12] Jin, W., Kohn, R. V., Singular perturbation and the energy of folds. *J. Nonlinear Sci.*, **10(3)** (2000), pp. 355–390.
- [13] Kohn, Slastikov, Another thin–film limit of micromagnetics. *submitted to Arch. Rat. Mech. Anal.*
- [14] Koslowski, M., Cuitiño, A. M., Ortiz, M., A phase-field theory of dislocation dynamics, strain hardening and hysteresis in ductile single crystals. *J. Mech. Phys. Solids*, **50(12)** (2002), pp. 2597–2635.
- [15] Kurzke, M., A nonlocal singular perturbation problem with periodic well potential. *ESAIM Control Optim. Calc. Var.*, **12(1)** (2006), pp. 52–63 (electronic).
- [16] Melcher, C., Micromagnetic treatment of Néel walls. *Arch. Rat. Mech.*, **168** (2003), pp. 83–113.
- [17] Melcher, C., Logarithmic lower bounds for Néel walls. *Calc. Var. Partial Differential Equations*, **21(2)** (2004), pp. 209–219.
- [18] Otto, F. Cross-over in scaling laws: a simple example from micromagnetics. In *Proceedings of the International Congress of Mathematicians, Vol. III (Beijing, 2002)*, pp. 829–838, Beijing, 2002. Higher Ed. Press.
- [19] van den Berg, H. A. M., Self-consistent domain theory in soft ferromagnetic media. ii. basic domain structures in thin film objects. *J. Appl. Phys.*, **60** (1986), pp. 1104–1113.
- [20] Verhulst, F., *Nonlinear Differential Equations and Dynamical Systems*. Springer–Verlag (1989).